Hindawi
Journal of Nanomaterials
Volume 2017, Article ID 8707289, 14 pages
https://doi.org/10.1155/2017/8707289

Research Article

Low Temperature Oxidation of Carbon Monoxide over Mesoporous Au-Fe_2O_3 Catalysts

Abdulmohsen Ali Alshehri and Katabathini Narasimharao

Department of Chemistry, Faculty of Science, King Abdulaziz University, P.O. Box 80203, Jeddah 21589, Saudi Arabia

Correspondence should be addressed to Abdulmohsen Ali Alshehri; aayalshehri@kau.edu.sa

Received 5 March 2017; Revised 23 May 2017; Accepted 6 June 2017; Published 10 July 2017

Academic Editor: Felipe A. La Porta

Low temperature active and stable mesoporous Au (0.1, 0.2, 0.5, and 1.0 wt.%) supported α-Fe_2O_3 catalysts were prepared via deposition-precipitation method. The H_2-pretreated catalyst with 0.5 wt.% Au loading offered CO conversion of 100% at 323 K and showed continual activity for at least 120 h. X-ray diffraction and transmission electron microscopy analysis indicate that Au species were highly dispersed as nanoparticles (20–40 nm) on the surface of α-Fe_2O_3 support even after thermal treatment at 773 K. The N_2-physisorption measurements show that the synthesized α-Fe_2O_3 support and Au-Fe_2O_3 nanocomposites possessed mesopores with high specific surface area of about 158 $m^2\ g^{-1}$. X-ray photoelectron spectroscopy and H_2-TPR results reveal that the Au species exist in metallic and partially oxidized state due to strong interaction with the support. Effective Au-Fe_2O_3 interaction resulted in a high activity for Au nanoparticles, locally generated by the thermal treatment at 773 K in air.

1. Introduction

The activity of humans in the world led to massive production of carbon monoxide (CO), starting from wood burning for warming houses and utilization of fossil fuels for electricity production, automobile engines, and industrial chemical combustion, which involves incomplete oxidation of carbon compounds [1]. In environmental aspects, CO is a highly toxic gas; high concentration of CO in the atmosphere is hazardous for lives, and it causes many illnesses, suffocation, and sudden death [2]. CO is converted to CO_2 which is a less toxic and natural gas that exists in the air; CO_2 is also a feedstock for methanol production, which in turn is used to produce many chemical compounds that are valuable for human life, such as plastics [3]. In general, the catalyst efficiency in CO oxidation is determined by its ability to oxidize CO to CO_2 fully at a low reaction temperature. For instance, the catalytic converter used in automobiles exhaust is proposed to oxidize CO at a temperature lower than 373 K, as it mainly contains traces of precious metals, for instance, palladium, platinum, and rhodium [4]. Au supported catalyst was demonstrated as a highly active catalyst [5]; precious metals are expensive; therefore, enhancement of the support properties plays a key role in catalytic activity, where a small amount of precious metal is doped on a large amount of support. It was reported that transition-metal oxides such as Fe_2O_3, TiO_2, Co_3O_4, and NiO are suitable supports [6]. The bulk α-Fe_2O_3 is a reducible support to provide a large amount of active sites; several researchers used α-Fe_2O_3 as a support for CO oxidation. We recently synthesized Ag-Fe_2O_3 nanocomposites and utilized them as catalysts for CO oxidation [7]. It was reported that α-Fe_2O_3 possessed an advantage in that it has a long lifetime because it could resist poisoning from CO_2 [8]. Many research groups [9–13] utilized Au supported iron oxide materials as a catalyst for CO oxidation. However, the controlled synthesis of Au metal oxide nanocomposites still faces tremendous challenges [14].

The preparation method of α-Fe_2O_3 support shows a significant change in support properties such as particle size, morphology, and surface area and their interaction with active metals. Synthesized α-Fe_2O_3 nanoparticles showed a much higher activity than microcrystalline α-Fe_2O_3 for CO oxidation; in other words, α-Fe_2O_3 could be fabricated in a desired morphology to obtain an efficient catalyst [15].

Mesoporous support (in which the pore size ranges between 2 and 50 nm) has an advantage to obtain good dispersion of active metal nanoparticles; the mesopores are responsible for capillary condensation and allow active metal nanoparticles to disperse more into the wall of pores [16]. Mesoporous Fe_2O_3 was prepared by different methods using templates, such as cellulose nanocrystals template [17] and SBA-15 [18]. Park and Lee [12] observed that oxidized gold species are important for CO oxidation and the authors concluded that the oxidized gold species were more active than metallic gold. Further, different opinions were reported with respect to the active catalyst that contained both Au atoms and ions [19, 20]. However, strong evidence of the oxidation states of Au for achieving high activity is one of the major issues that has not yet been resolved.

In this work, we aim to synthesize nanosized mesoporous Au-Fe_2O_3 composites and use them as catalysts for CO oxidation at low reaction temperatures. We also made an effort to study the physicochemical properties of the catalysts and correlate the properties with catalytic CO oxidation activity.

2. Experimental

2.1. Preparation of Mesoporous α-Fe_2O_3 Nanomaterials. Single-crystalline mesoporous α-Fe_2O_3 nanomaterials were obtained by reacting $Fe(NO_3)_3{\cdot}9H_2O$ with $NH_4H_2PO_4$ under hydrothermal conditions [21]. Typically, 1.0 g of $Fe(NO_3)_3{\cdot}9H_2O$ was added to 10 mL of 0.1 N aqueous $NH_4H_2PO_4$ solution. The added $Fe(NO_3)_3{\cdot}9H_2O$ was hydrolyzed within a few minutes, and a brown colored precipitate was formed. The obtained precipitate was stirred for 1 h and then transferred into an autoclave lined with a Teflon vessel. Then, the autoclave was heated in an electric oven at a temperature of 353 K for 12 h. After the hydrothermal treatment, the precipitate was washed with distilled water four times, dried in a vacuum oven at 373 K for 12 h, and calcined at 773 K for 2 h.

2.2. Preparation of Au-Fe_2O_3 Nanocomposites. Gold was loaded on synthesized Fe_2O_3 support via the deposition-precipitation method. In this method, the aqueous suspension containing 1.0 g of the support material was heated in a water bath at 373 K and the pH value of the solution was adjusted to 9.0 by adding 1 N NH_4OH solution. A $HAuCl_4$ solution corresponding to Au loading (0.1, 0.2, 0.5, and 1.0 wt.%) was poured into the suspension. Additional NH_4OH solution was added dropwise to the suspension to keep the pH value stable. After stirring for 30 min and aging for 2 h at room temperature, the precipitate was filtrated and washed several times with deionized water until no Cl^- was detected by a 0.25 mol L^{-1} $AgNO_3$ solution. The resultant precipitate was dried at 393 K for 3 h and then calcined at 773 K for 4 h. The catalysts were denoted as xAu-Fe, where x represents the Au loading.

2.3. Characterization. The elemental composition of the catalysts was performed using ICP-AES, Optima 7300DV (PerkinElmer Corporation, USA) instrument. The sample preparation procedure for elemental analysis and a detailed description of the experimental procedure were described in our previous publication [22].

The powder X-ray diffraction measurements for the samples were performed using Bruker D8 Advance target diffractometer. The XRD patterns were obtained using Cu Kα radiation (λ = 1.5405 Å) at 40 kV and 40 mA. The identification of phases presented in the samples and crystallite sizes of iron oxide and gold metal were calculated using Scherrer equation as described in our previous publication [22].

Transmission electron microscopy (TEM) and high-resolution TEM images of the samples were obtained using a Philips CM200FEG microscope equipped with a field emission gun operated at 200 kV. Diffuse reflectance UV-Vis spectra for all the samples were collected using a Thermo Scientific evolution 600 UV-visible spectrophotometer conjugated with an integrating sphere in the wavelength range of 200–800 nm.

The textural properties of the synthesized samples were determined from N_2 adsorption-desorption measurements at 77 K carried out using Quantachrome NOVA 3200e automated gas adsorption system. A detailed procedure was described in our previous publication [22] to determine the specific surface area, pore volume, and average pore radius of the samples. The X-ray photoelectron spectroscopy measurements for all the samples were carried out using a SPECS GmbH XPS instrument. A standard dual anode excitation source with Mg Kα (1253.6 eV) radiation was used at 13 kV and 100 W. H_2-temperature programmed reduction profiles for all the catalyst samples were collected using Quantachrome CHEMBET-3000 instrument. More details of the experimental procedures used in this work can be found in our previous publications [7, 22].

2.4. Catalytic Oxidation of Carbon Monoxide. Catalytic activity measurements for CO oxidation were carried out using a fixed-bed reactor at atmospheric pressure. Quartz spheres (0.5 g) were used to dilute the Au-Fe_2O_3 catalyst (0.5 g) in a quartz reactor. Prior to the activity tests, the catalysts were treated with 10% H_2/N_2 (100 mL min^{-1}) at 353 K for 1 h. After the catalysts were cooled down to 273 K under N_2 (100 mL min^{-1}), the feed gas containing 100 ppm CO balanced with compressed air was passed through the reactor at 1000 mL min^{-1}. The reaction temperature, measured with a thermocouple, was increased from 273 K to 333 K. Online gas chromatograph (Agilent) with a TCD detector was employed to measure the reactor inlet and outlet gas streams. TDX-01 column (2 m × 4 mm) was used to separate O_2, CO, and CO_2.

The conversion of CO was by change in CO concentration:

$$\text{CO conversion (\%)} = \left\{[\text{CO}]_{\text{inlet}} - \frac{[\text{CO}]_{\text{outlet}}}{[\text{CO}]_{\text{inlet}}}\right\} \times 100. \quad (1)$$

3. Results and Discussion

The XRD patterns for pure iron oxide and Au-Fe nanocomposite samples are shown in Figure 1. The bulk Fe_2O_3 sample

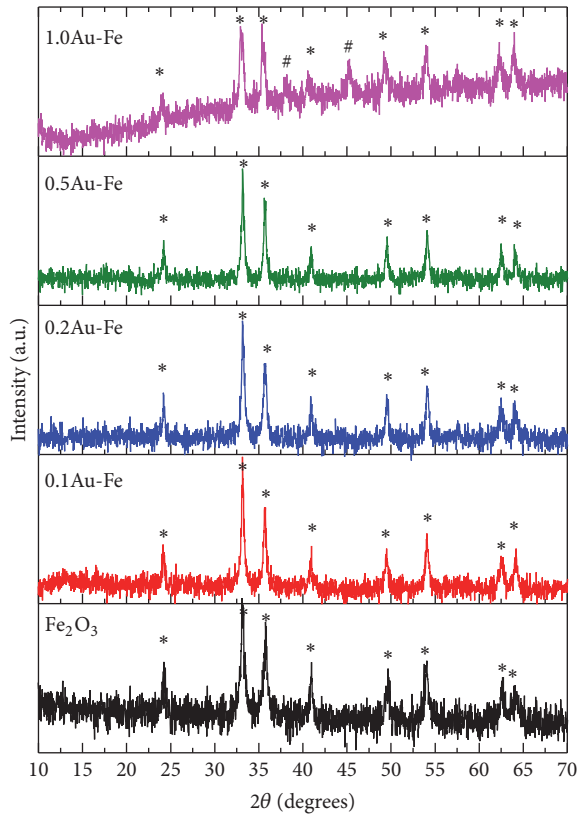

Figure 1: XRD patterns of the samples.

calcined at 773 K showed diffraction peaks at $2\theta = 24.4^\circ, 33.5^\circ, 36.0^\circ, 41.1^\circ, 49.8^\circ, 54.7^\circ, 57.3^\circ, 62.7^\circ$, and 64.4° corresponding to (012), (104), (110), (113), (024), (116), (122), (214), and (300) planes, respectively. These peaks are clearly indexed to α-Fe_2O_3 phase [JCPDS number 01-1030]. XRD peaks for the α-Fe_2O_3 sample are significantly broader than those for the micrometer sized sample, indicating that the sample possessed a very small particle size. It is also noteworthy that the synthesized sample does not show any diffraction peaks corresponding to any other crystalline phase, indicating the purity of the sample. XRD patterns of the Au-Fe nanocomposites with 0.1, 0.2, and 0.5 wt.% Au loadings showed only characteristic diffraction peaks of α-Fe_2O_3. Neither Au oxide nor metallic Au was detected at lower Au loading (<1.0 wt.%). This is possibly due to high dispersion of Au particles on Fe_2O_3 support in lower loadings. The decrease of intensity of diffraction peaks due to Fe_2O_3 clearly indicates the decrease of crystallinity of the sample with the increase of Au loading. Additional diffraction peaks can be seen for the 1.0Au-Fe sample: diffraction peaks at $2\theta = 38.2^\circ$ and $2\theta = 44.5^\circ$ corresponding to (111) and (200) planes [23] for metallic Au crystallites for the 1.0Au-Fe sample.

The TEM analysis was used to determine the morphology and size of the Au and Fe_2O_3 phases presented in the samples. The TEM images of the Au-Fe nanocomposite samples are presented in Figure 2. It was observed that the synthesized α-Fe_2O_3 sample possessed some small cylindrically shaped nanoparticles of about 15–25 nm diameter and 150–200 nm length and also many large particles which are composed of several small cylindrically shaped nanoparticles.

Table 1: Crystallite sizes of the samples determined from XRD and TEM measurements.

Catalyst	Crystallite size (nm)			
	XRD		TEM	
	Fe_2O_3	Au	Fe_2O_3	Au
α-Fe_2O_3	55 ± 0.3	—	45	—
0.1Au-Fe	55 ± 0.4	—	45	20
0.2Au-Fe	54 ± 0.4	—	45	20
0.5Au-Fe	52 ± 0.3	—	45	15
1.0Au-Fe	45 ± 0.4	40 ± 0.3	42	40

This is possibly due to calcination of the samples at a high reaction temperature leading to several particles bundling together via hydrophilic interactions. Some aggregated spherically shaped Fe_2O_3 nanoparticles of size around 50 nm are also observed along with the cylindrically shaped nanoparticles. The presence of large crystalline particles indicates the formation of polycrystallites, due to the high temperature calcination (773 K). No clear differences in shape, size, and dispersion of Au are observed in the 0.1Au-Fe and 0.2Au-Fe catalysts. However, we must take into account the fact that the loading of Au in these samples is very low and it makes the detection of Au particles difficult due to the low mass and diffraction contrast. TEM images of 0.5Au-Fe and 1.0Au-Fe samples clearly show thick black spherical grain of Au metal on the α-Fe_2O_3 surface with a size of about 45 nm. Large pores are observed in between the α-Fe_2O_3 particles, which is further confirmed by N_2 adsorption analysis and discussed in a later part of the Results and Discussion.

The particle size for all the samples was calculated using Scherrer's equation and XRD peak broadening, as shown in Table 1. The half widths of (104) peak of α-Fe_2O_3 at $2\theta = 33.5^\circ$ and of (111) peak of Au at $2\theta = 38.2^\circ$ (both Cu Kα) were used. Scherrer's equation gives the average size in the order of 45 nm for the Fe_2O_3 and 40 nm for the Au in case of 1.0Au-Fe sample. The XRD determined crystallite sizes of α-Fe_2O_3 and Au were higher than the crystallite size measured by TEM analysis. Nonuniform particle size distribution could be a reason for such behavior. The average crystal size of α-Fe_2O_3 was calculated to be 55 nm. The responsible species for the catalytic properties of Au supported catalysts is not clear yet although it was suggested that the interface structures between the Au nanoparticle and metal oxide support act as active sites [24]. In order to understand the interface structure, we carried out high-resolution transmission electron microscopy (HRTEM) analysis for 0.5Au-Fe and 1.0Au-Fe samples. The HRTEM images of both of these samples are shown in Figure 3. It can be seen that there are two lattice fringes with lattice spacings of 0.235 nm and 0.270 nm corresponding to the Au (111) and Fe_2O_3 (104) planes from different grains, respectively [25], which further confirm the synthesis of Au-Fe_2O_3 nanocomposite.

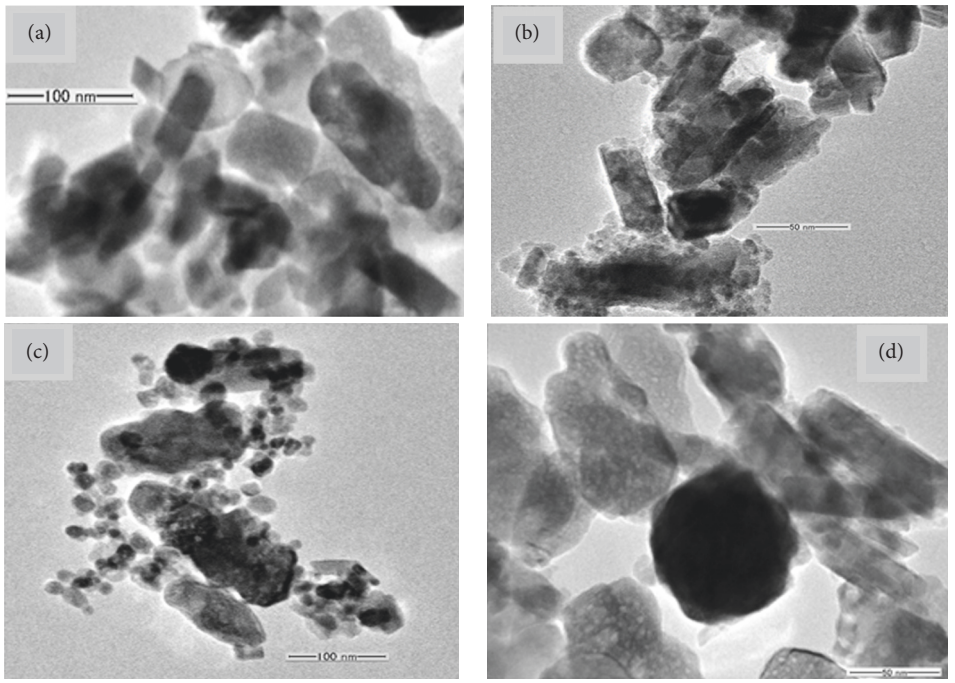

Figure 2: TEM images of (a) 0.1Au-Fe, (b) 0.2Au-Fe, (c) 0.5Au-Fe, and (d) 1.0Au-Fe samples.

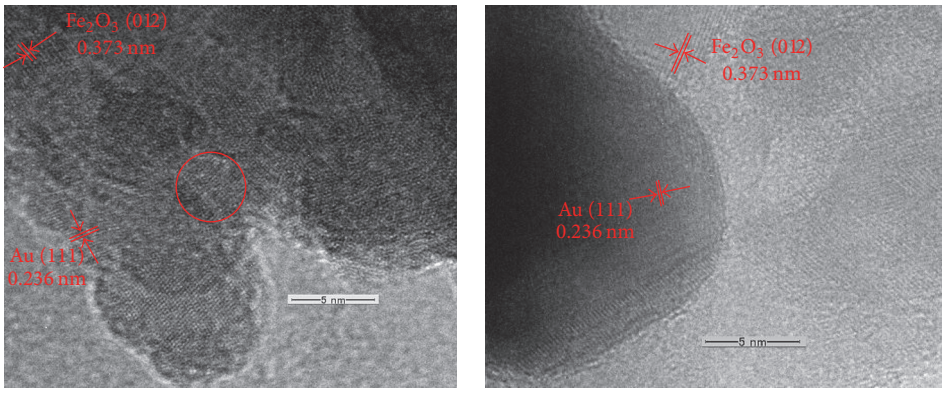

(a) (b)

Figure 3: HRTEM images of (a) 0.5Au-Fe and (b) 1.0Au-Fe catalysts.

In case of 1.0Au-Fe sample, a large size Au particle was observed, which might be formed from several smaller particles, and it was deposited on the plain of Fe_2O_3 support. The crystal lattices of Au (111) and Fe_2O_3 (104) are distinct and without strong interaction with each other. On the other hand, in the 0.5Au-Fe sample, it can be seen that the Au crystal lattices were overlapped with each other and the Au particles were surrounded with crystalline Fe_2O_3 and a distinct interface between Au particles and Fe_2O_3 formed.

The UV-Vis diffuse reflectance spectra of calcined Fe_2O_3 and Au-Fe nanocomposites are shown in Figure 4. It was reported that iron oxides generally show three kinds of optical transitions. The peaks between 200 and 400 nm mainly result from the ligand to metal charge transfer transitions and partly from the contribution of the Fe^{3+} ligand-field transitions. The region between 400 and 600 nm is considered to be a result of pair excitation processes, possibly overlapping the contributions of ligand-field transitions [7]. He et al. [26] reported that the peaks in the 600–750 nm and 750–900 nm regions could be due to the *d-d* transitions. It is widely known that deposition of the Au on any support leads to a broad absorption band in the range of 500–570 nm and this contribution can be assigned to the well-known plasmon resonance of Au nanoparticles [27].

In case of Au-Fe_2O_3 nanocomposite samples, the contribution from Au nanoparticles was masked by the extended absorption of α-Fe_2O_3 in the visible region [28]. However, an increase in the broadness of the Au plasmon absorption band was observed with the increase of Au loading from 0.1 wt.% to 1.0 wt.%, although Au-Fe nanocomposite samples

Table 2: Elemental composition and textural properties of the catalysts.

Catalyst	Surface area ($m^2\,g^{-1}$)	Pore volume ($cc\,g^{-1}$)	Pore radius (Å)	Bulk elemental composition (ICP analysis)			Surface elemental composition (XPS analysis)		
				Au	Fe	Au/Fe	Au	Fe	Au/Fe
Fe_2O_3	172 ± 5	0.316	87.7	—	41.5	—	—	41.4	—
0.1Au-Fe	168 ± 3	0.314	87.6	0.09	41.4	0.002	0.1	41.4	0.002
0.2Au-Fe	159 ± 3	0.273	87.7	0.18	38.4	0.005	0.2	38.6	0.004
0.5Au-Fe	142 ± 4	0.228	87.6	0.43	36.6	0.011	0.3	36.8	0.008
1.0Au-Fe	118 ± 3	0.145	156.4	0.87	32.2	0.027	0.5	32.6	0.015

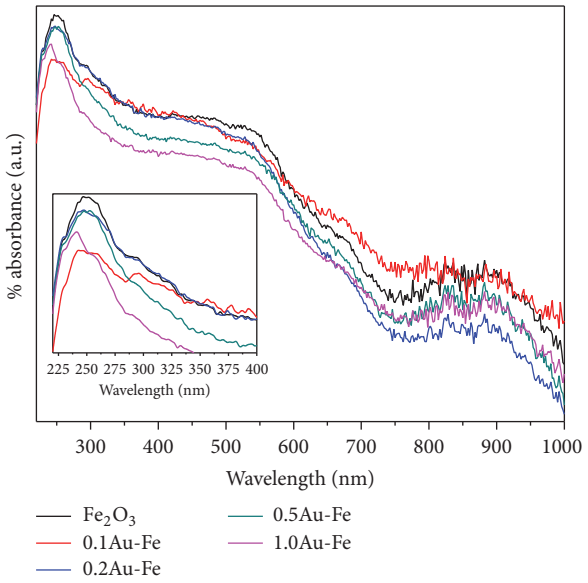

Figure 4: UV-Vis diffuse reflectance spectra for all the samples.

display weak plasmon resonance. Furthermore, a red shift was observed as Au nanoparticles agglomerate on the Fe_2O_3 surface in case of 1.0Au-Fe sample owing to the relatively big particle size and interparticle interactions. It is possible that the adsorption of oxygen on Au surfaces leads to the formation of surface oxide and forms Fe-Au interactive species in the nanocomposite samples.

The textural properties of calcined α-Fe_2O_3 and Au-Fe nanocomposites were studied by the N_2-physisorption measurements. The N_2 adsorption-desorption isotherms of all the samples are shown in Figure 5. For all the samples, the isotherms are identified as type III according to the IUPAC classification, which is a typical characteristic of macroporous materials [29], and a clear H3-type hysteresis loop is observed, thus indicating the presence of plate-like particles giving rise to slit-shaped pores [30]. The hysteresis loop for the 0.1Au-Fe, 0.2Au-Fe, and 0.5Au-Fe samples is similar to the Fe_2O_3 support, thus indicating that the deposition of Au in low loadings did not modify the macroporous nature of the support. In case of 1.0Au-Fe sample, a similar hysteresis shape was observed; however, the relative pressure where the condensation step occurs shifted to higher P/P^0 values.

The BET surface area, average pore diameter, and pore volume of all the samples estimated from their respective adsorption-desorption isotherms are given in Table 2. The BET surface area of the calcined macroporous α-Fe_2O_3 is $72\,m^2\,g^{-1}$, which is more than 12 times higher than the commercial α-Fe_2O_3 ($6.0\,m^2\,g^{-1}$). The pore volume of the α-Fe_2O_3 was found to be $0.316\,cm^3\,g^{-1}$. A decrease of surface area was observed with the increase of Au loading; this is probably due to the fact that Au deposition onto α-Fe_2O_3 makes the pore walls lower than pure Fe_2O_3, which is reflected in their surface areas and also confirmed by their respective pore volume and pore radius data.

The pore size distribution (PSD) was obtained by Barrett-Joyner-Halenda (BJH) method as shown in Figure 5(b). The porous Fe_2O_3 shows unimodal pore size distribution with predominant pore radius of around 87.7 Å. It is likely that some Au nanoparticles crystallized inside the pores of Fe_2O_3 support during the thermal treatment, thus partially blocking them from the outside, and as a consequence, the mean pore size was shifted to higher values.

X-ray photoelectron spectroscopy (XPS) analysis was utilized to determine the electronic states of elements and composition of the Au-Fe nanocomposites. The XPS spectra of Fe *2p*, Au $4f$, and O 1*s* of Au-Fe nanocomposite samples are shown in Figure 6. From the figure, it is clear that the Au $4f_{7/2}$ peak is weak and Au $4f_{5/2}$ is not clearly observed for the 0.1Au-Fe sample due to its low Au loading. However, both Au $4f_{7/2}$ and Au $4f_{5/2}$ peaks were clearly observed after the increase of Au loading (beyond 0.2 wt.%). It was reported that the $4f_{7/2}$ and $4f_{5/2}$ binding energy values for metallic Au^0 are 84.1 eV and 87.7 eV. The Au $4f_{7/2}$ binding energies for the oxidized Au^+ and Au^{3+} ions are 85.6 eV and 86.5 eV, respectively [31]. After peak deconvolution of the Au $4f$ energy regions, single Au $4f_{7/2}$ and Au $4f_{5/2}$ were observed at 83.4 eV and 87.2 eV, respectively, for 0.1Au-Fe, 0.2Au-Fe, and 0.5Au-Fe samples. The binding energy value of Au $4f_{7/2}$ observed for these samples is lower than the bulk gold (84.1 eV) indicating the formation of Au-Fe_2O_3 interactive species [11]. A similar observation was reported in the literature [32, 33]. Further, the binding energy of Au $4f$ peaks in the 0.2Au-Fe sample is slightly lower than in the 0.1Au-Fe and 0.5Au-Fe samples. There is probably a stronger interaction between the Au particles and the Fe_2O_3 support in 0.2Au-Fe than the other two samples.

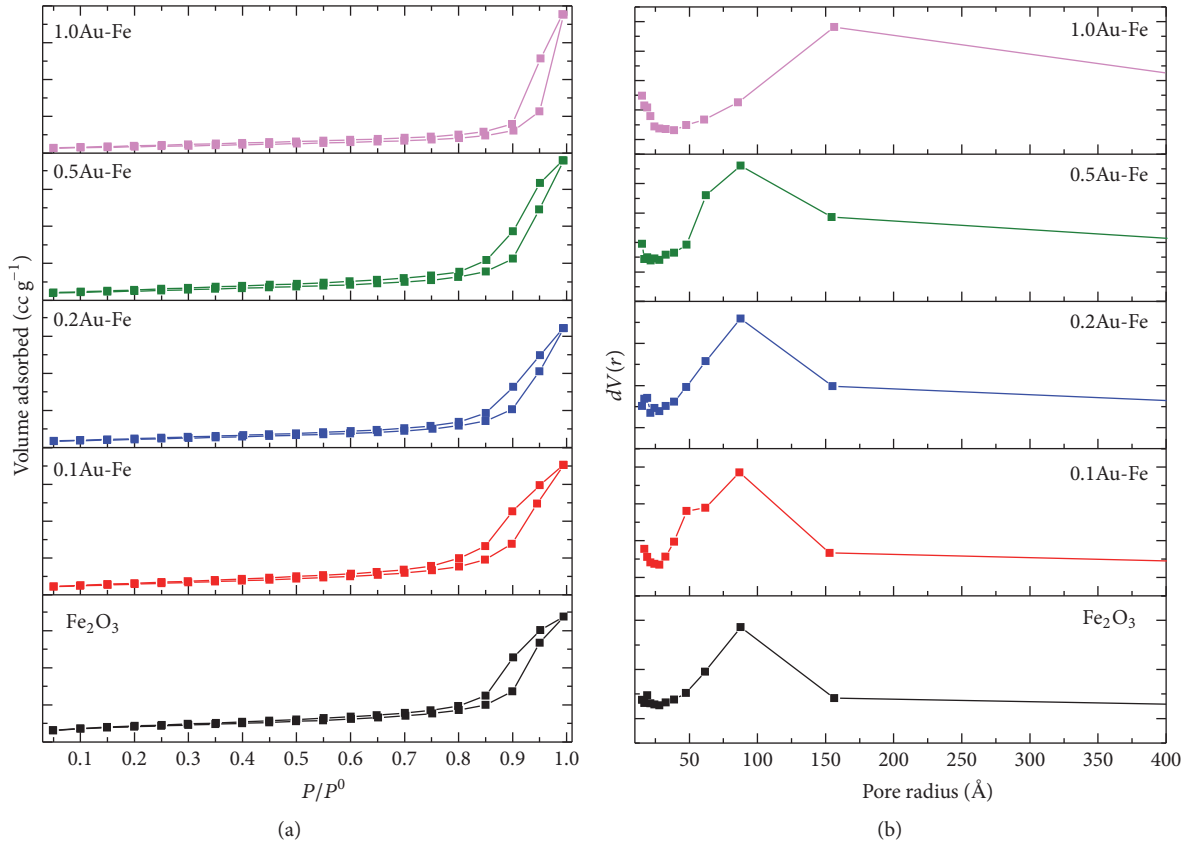

FIGURE 5: (a) N_2 adsorption-desorption isotherms. (b) Pore size distribution patterns of all the samples.

It is interesting to note that, after deconvolution of the Au $4f_{7/2}$ energy regions for the 1.0Au-Fe sample, two components at 83.0 eV (I) and 84.3 eV (II) due to metallic Au and oxidized surface Au species were observed [34]. Lin and Chen [35] also observed two distinct peaks of Au supported iron oxide catalysts. The binding energy value of Au $4f_{7/2}$ peak (II) is higher than that of Au^0 but lower than that of Au^+ and Au^{3+}. This observation suggests that the oxidized Au species are in the form of $Au^{\delta+}$, which is a transition state between Au^0 and Au^+ due to the interaction between nanosized Au particles and the Fe_2O_3 support [36]. The XRD patterns of 0.1Au-Fe, 0.2Au-Fe, and 0.5Au-Fe samples did not show any diffraction peaks corresponding to metallic Au, but the XPS analysis of these samples shows the presence of metallic Au on the support surface. One possible explanation is that the metallic gold formed on the support surface remains largely amorphous in these low loading samples, as amino or nitroso complexes of gold generally get precipitated during the precipitation-deposition method under basic conditions. Upon heating at 393 K, amino or nitroso complexes of gold start to decompose to metallic gold and gold oxides when we calcine the material at 773 K [11].

It was observed that Fe_2O_3 sample showed Fe $2p_{3/2}$ peak maxima at 710.6 eV (not shown in Figure 6); some differences were observed in the Fe $2p_{3/2}$ binding energy values for Au-Fe nanocomposite samples. The $2p_{3/2}$ peak was shifted to higher binding energies (711.6 eV for 0.1, 0.2, and 0.5 wt.% Au and 711.9 eV for 1.0 wt.% Au), indicating that the Fe oxidation state of surface iron species is sensitive to the Au composition. Brundle [37] reported that, in bulk iron oxides, Fe (III) has a $2p_{3/2}$ binding energy of 711 eV, and the $2p_{3/2}$ binding energy of Fe(II) is centered at 709.7 eV. The Fe $2p$ deconvoluted spectra of all the Au-Fe samples also showed a minor peak located in between 709.2 eV and 708.7 eV and this peak can be attributed to Fe species with lower oxidation state. The appearance of this peak is due to the formation of Au-Fe interactive species on the support surface. The contribution of this peak to the 0.2Au-Fe sample was 2.2% and increased to 4.3% after the loading was increased to 0.5 wt.%. A further increase of Au loading to 1.0 wt.% caused a decrease in the concentration of this peak to 3.6%. These observations led to the conclusion that the Au nanoparticles are interacting with Fe_2O_3 due to increased dispersion of the Au metal nanoparticles on the surface of Fe_2O_3 support. This statement is supported by the increased Au/Fe atomic ratio derived from XPS measurements (Table 2). It is also interesting to note that bulk Au/Fe ratio determined from ICP-AES analysis is higher than Au/Fe ratio derived from XPS analysis results. This observation indicates that the part of the deposited Au is transported into the spaces existing in between the Fe_2O_3 nanoparticles.

The deconvoluted O 1*s* spectra for all the samples are shown in Figure 6. Three different peaks can be clearly seen in the spectra, which correspond to three different oxygen

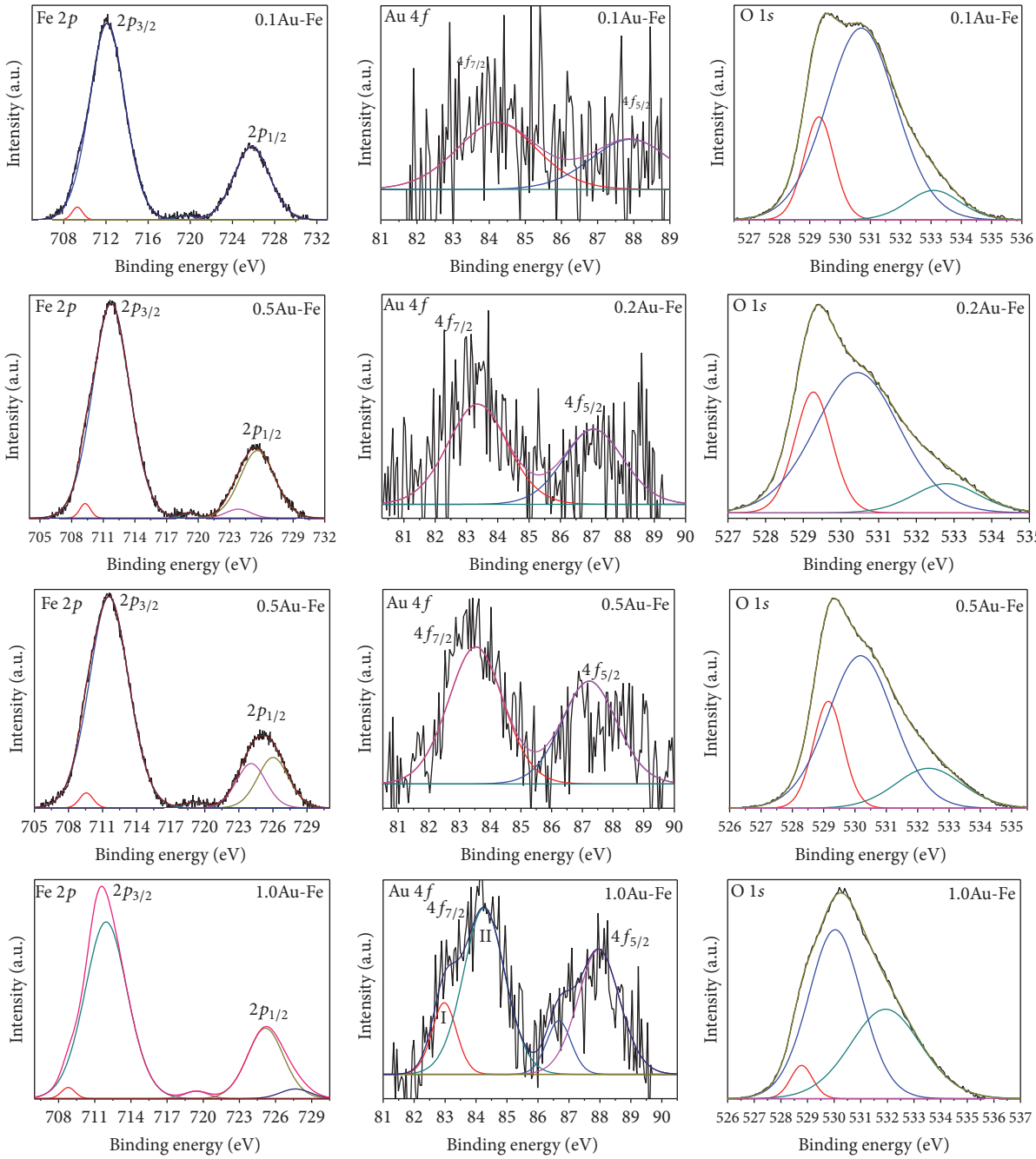

Figure 6: XPS spectra for all the samples.

species. The 0.1Au-Fe sample showed peaks at 529.3 eV, 531.0 eV, and 533.1 eV. The peaks at 531.0 eV and 529.3 eV can be attributed to oxygen in Fe_2O_3 and Au-Fe_2O_3 interactive species, respectively, while the other peak at 533.1 eV can be related to oxygen in the electrophilic state adsorbed on Au metal [38]. The relative proportion of the area under the XPS peaks was changed with Au loading (Table S1). The contribution due to the XPS peak at 533.1 eV was increased with the increase of Au loading from 0.1 to 1.0 wt.%; this observation indicates the increase of Au metal concentration on the Fe_2O_3 surface. On the other hand, the contribution due to the O 1*s* peak at 529.3 eV was increased up to 0.5 wt.% but decreased upon further increase to 1.0 wt.%. The XPS results are in accordance with the observations from the TEM analysis, and Au-Fe nanocomposites possess two types of (Au metal and Au-Fe interactive) species and the extent of formation of these species is dependent on the Au loading over the Fe_2O_3 support.

H_2-TPR analysis for all the samples was performed to study the reduction behavior and nature of Au-Fe interaction

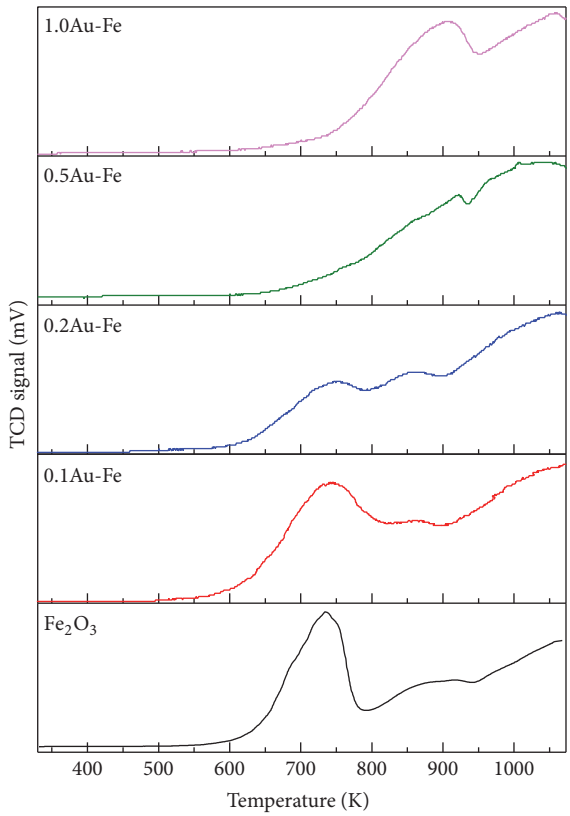

FIGURE 7: H_2-TPR patterns for all the samples.

in the Au-Fe nanocomposites. Figure 7 shows the H_2-TPR spectra of α-Fe_2O_3 and Au-Fe nanocomposite samples calcined at 773 K. The H_2-TPR spectrum of α-Fe_2O_3 showed a broad peak that started at 623 K attributed to the reduction of Fe_2O_3 to Fe_3O_4 (T_{max} = 723 K) and the other extensive peaks at temperatures beyond 773 K. It was reported that, in the literature [39], the H_2-TPR peak that appeared at 573 K can be attributed to the reduction of the hydroxylated Fe_2O_3 species and the peak at ≈673 K can be attributed to the reduction of Fe_2O_3 to Fe_3O_4. The reduction of Fe_3O_4 to FeO occurs at ≈873 K and finally the reduction to Fe^0 happens above 1073 K. We can also observe that the high temperature peak does not reach the baseline in the H_2-TPR profile of bulk Fe_2O_3 sample even at 1073 K, which means the reduction was continued above this temperature.

The H_2-TPR patterns for the 0.1Au-Fe and 0.2Au-Fe nanocomposite samples are very similar to the bulk Fe_2O_3 sample; however, deposition of a small amount of Au resulted in a shift in T_{max} of the peak due to reduction of FeO to Fe and also the high temperature peak started reaching the baseline in case of 0.2Au-Fe sample. This observation reveals that deposition of small amounts of Au could enhance the reduction of Fe_2O_3. On the other hand, the H_2-TPR spectra of 0.5Au-Fe and 1.0Au-Fe samples substantially differ from the other samples. Increasing of Au loading to 0.5 and 1.0 wt.% resulted in the disappearance of the reduction peak at T_{max} = 723 K (reduction of Fe_2O_3 to Fe_3O_4). Carabineiro et al. [40] reported similar results that Au supported Fe_2O_3 catalysts showed two reduction peaks above 800°C, which could be due to the reduction of Fe_3O_4 to FeO (or of FeO to Fe). The deposition of a larger amount of Au leads to the formation of agglomerated Au nanoparticles, which interact with Fe_2O_3 leading to a shift in reduction temperature. Venugopal and Skurrell [41] also observed a shift in reduction temperature due to the interaction between the Au species and iron oxide support.

The H_2 uptake values during the different reduction stages are calculated from integrating the area of the reduction peaks, which are tabulated in Table S2. The overall H_2 consumption of the reduction peaks can be assigned to the reduction of α-Fe_2O_3 to Fe_3O_4 and also the reduction of Fe_3O_4 to Fe. In the two stages of reduction, Fe_2O_3 reacted with hydrogen based on the following reactions.

$$3Fe_2O_3 + H_2 \rightarrow 2Fe_3O_4 + H_2O;\ \text{mol } H_2/\text{mol Fe} = 0.166 \text{ for complete reduction}$$

$$Fe_3O_4 + 4H_2 \rightarrow 3Fe + 4H_2O;\ \text{mol } H_2/\text{mol Fe} = 1.33 \text{ for complete reduction}$$

The H_2 consumption value observed for bulk Fe_2O_3 is consistent with the theoretical value. However, the overall H_2 consumption observed for Au-Fe nanocomposite samples is higher than the stoichiometric amount required to reduce all the Fe presented in the catalyst, indicating that some degree of surface reduction of catalyst takes place at high temperatures as a result of Au-Fe interaction in these catalysts.

A fixed-bed catalytic reactor was used to evaluate the catalytic activity of synthesized bulk Fe_2O_3 and Au-Fe nanocomposite samples. The reactions were conducted at the temperature range of 273–333 K isothermally. Figures 8(a) and 8(b) show the catalytic activity in CO oxidation of calcined and H_2-pretreated catalysts, respectively. In case of calcined catalysts (Figure 8(a)), 100% CO conversion was observed for 0.5Au-Fe catalyst at 313 K, whereas CO conversion levels corresponded to 97%, 92%, and 41% for 1.0Au-Fe, 0.2Au-Fe, and 0.1Au-Fe catalysts, respectively. The bulk Fe_2O_3 support did not show any CO conversion at the same temperature.

The CO oxidation catalytic activity results obtained for the H_2-pretreated catalysts are shown in Figure 8(b). At lower reaction temperatures, for instance, 283 K, the catalysts showed a very little difference in CO conversion (78%-0.1Au-Fe, 80%-0.2Au-Fe, 83%-0.5Au-Fe, and 78%-1.0Au-Fe). The CO conversion increased to 100% at 323 K for all Au-Fe nanocomposite samples. The much higher performances of the H_2-pretreated Au-Fe nanocomposite samples could be due to the well dispersed Au nanoparticles and Au-Fe_2O_3 interactive species [42]. It is known that the well dispersed Au nanoparticles could weaken C-O and O-O bonds after CO and O_2 adsorption, influencing the interaction between the surface and the adsorbents and favoring CO activation [43].

The influence of Au loading on CO conversion for the calcined and H_2-pretreated Au-Fe nanocomposite catalysts is shown in Figure 8. It is clear that the CO conversion was enhanced when the Au loading was increased from 0.1 to 0.5 wt.% and then decreased upon further increase of Au loading to 1.0 wt.%. In case of calcined Au-Fe nanocomposite

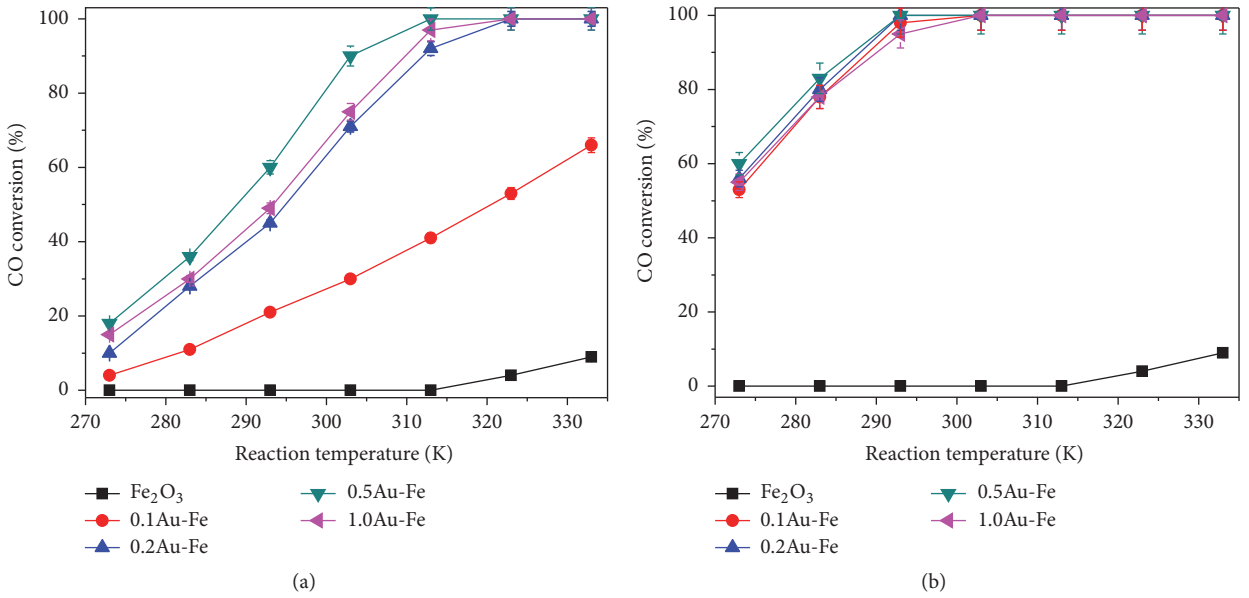

FIGURE 8: Catalytic activity in CO oxidation over (a) calcined Au-Fe and (b) H_2-treated Au-Fe nanocomposite catalysts (reaction conditions: weight of catalyst 0.5 g; total flow rate 1000 mL min^{-1}; feed composition 100 ppm CO/air; GHSV = 120,000 mL g^{-1} h^{-1}).

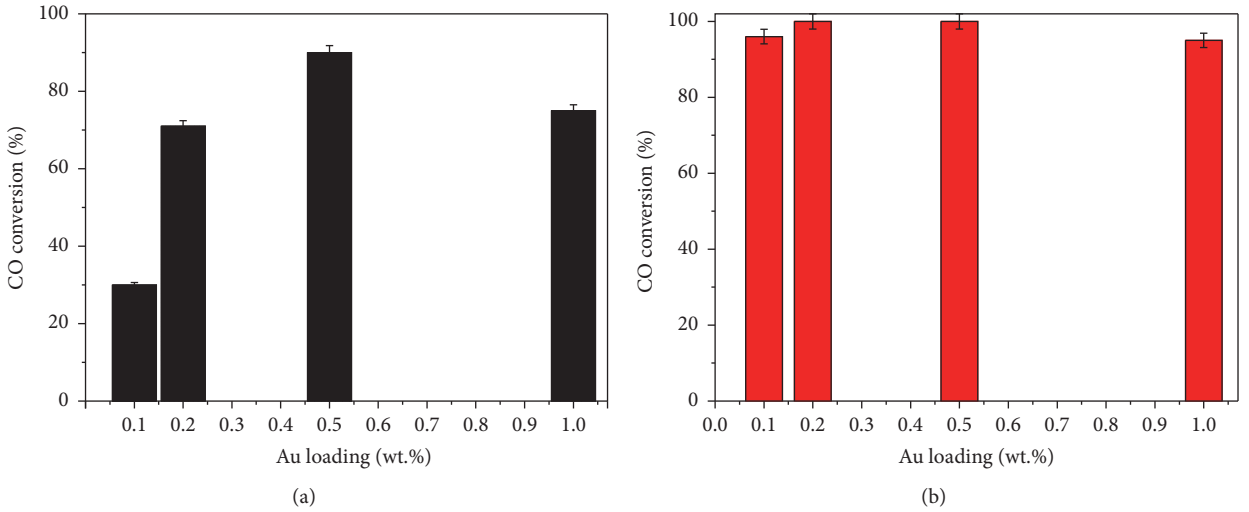

FIGURE 9: The influence of Au loading on CO conversion over the (a) calcined and (b) H_2-treated Au-Fe nanocomposite catalysts (reaction conditions: temperature 293 K; weight of catalyst 0.5 g; total flow rate 1000 mL min^{-1}; feed composition 100 ppm CO/air; GHSV = 120,000 mL g^{-1} h^{-1}).

samples, the CO conversion was increased from 30% to 90% when Au loading was increased from 0.1 wt.% to 0.5 wt.% but decreased to 75% upon further increase to 1.0 wt.%. A similar behavior was observed for H_2-pretreated catalysts. These results could be explained on the basis of low Au particle size, high dispersion of Au metal active sites for CO adsorption, and activation in case of 0.5Au-Fe catalyst, but agglomeration of Au nanoparticles was observed in case of 1.0Au-Fe catalyst.

Figure 9 represents the influence of GHSV on CO conversion over the calcined and H_2-pretreated 0.5Au-Fe catalyst; higher space velocity resulted in lower CO conversion and a similar behavior was observed in all the catalysts. This behavior is expected due to decreased reactants residence time on the catalyst surface with increased GHSV. In case of calcined 0.5Au-Fe catalyst, the CO conversion was decreased from 90% to 74% after the GHSV was increased from 60,000 mL g^{-1} h^{-1} to 120,000 mL g^{-1} h^{-1}; however, the extent of decrease is low in case of H_2-pretreated catalyst; the CO conversion was decreased from 100% to 93%. The CO oxidation activity results suggested that H_2 pretreatment greatly enhances the reaction rate.

A specific rate for CO oxidation for calcined 0.5Au-Fe catalyst was calculated and compared with reaction

Table 3: Specific rates of CO conversion and TOF data for Au supported catalysts from this work and literature reports.

Catalyst	Au loading (wt.%)	Specific rate $\times 10^{-2}$ ($mol_{CO}\ g_{Au}^{-1}\ h^{-1}$)	TOF $\times 10^{2}$ (s^{-1})	Reaction temperature (K)	Reference
Au/La_2O_3	0.5	4.0 ± 0	1.0 ± 0	298	[44]
Au/CeO_2	5.0	2.8 ± 0	4.7 ± 0	273	[45]
$Au/Fe\text{-}SiO_2$	2.0	0.7 ± 0	2.2 ± 0	273	[46]
Au/SiO_2	1.0	0.08 ± 0	0.03 ± 0	300	[47]
Au/Fe_2O_3-nanorod	0.5	3.6 ± 0	4.0 ± 0	303	[21]
Au/Fe_2O_3-Fluka	0.5	1.2 ± 0	2.1 ± 0	303	[21]
Au/Fe_2O_3-WGC	0.5	1.7 ± 0	2.5 ± 0	303	[40]
Au/Fe_2O_3-nanocomposite	0.5	12.4 ± 0.07	5.3 ± 0.05	293 ± 1	Present work

rates of different Au supported catalysts reported in the literature under similar reaction conditions (Table 3). The calcined 0.5Au-Fe catalyst showed a relatively high specific rate of $5.3 \times 10^{-2}\ mol_{CO}\ g_{Au}^{-1}\ h^{-1}$, which was more active than Au-La_2O_3 catalyst, which possessed a specific rate of $4.0 \times 10^{-2}\ mol_{CO}\ g_{Au}^{-1}\ h^{-1}$. The H_2 pretreatment enhanced the activity further, and the specific rate over the H_2-pretreated 0.5Au-Fe catalyst was increased to $12.4 \times 10^{-2}\ mol_{CO}\ g_{Au}^{-1}\ h^{-1}$, which was higher than that of the Au-Fe_2O_3 catalyst ($9.1 \times 10^{-2}\ mol_{CO}\ g_{Au}^{-1}\ h^{-1}$) prepared by the deposition-precipitation method [21, 44–47]. These results clearly indicate the superior catalytic activity of Au-Fe nanocomposite catalysts for CO oxidation.

The turnover frequencies (TOFs) were also calculated in order to gain an insight into the intrinsic activities of Au-Fe nanocomposite catalysts. The TOF of H_2-pretreated 0.5Au-Fe catalyst was $0.038\ s^{-1}$, exhibiting a significantly higher activity than that of calcined 0.5Au-Fe catalyst (TOF = $0.012\ s^{-1}$). The TOF of the H_2-pretreated 0.5Au-Fe catalyst was comparable to that of the Au/CeO_2 catalyst (TOF = $0.047\ s^{-1}$) [45] and the commercial Au/Fe_2O_3 catalyst (TOF = $0.04\ s^{-1}$) [21]. The TOF values of H_2-pretreated Au-Fe nanocomposite catalysts are higher than of the nanosized Au-Fe_2O_3 catalysts reported in the literature [21]. The enhanced activity of the catalyst could be attributed to the small size of the synthesized Au nanoparticles [48] and also the synthesized nanosized mesoporous Fe_2O_3 support possessed a high surface area. As a result, there is an increase in the amount of active sites for the CO_2 to adsorb. The oxygen adsorbs to the support and dissociates [49]. The stability of most active catalysts among the investigated samples was tested at 293 K and the time on stream analysis of the 0.5Au-Fe sample is shown in Figure 10. The CO conversion was readily decreased from 60% to 53% for 0.5Au-Fe calcined catalyst after 3 h and it was further decreased to 50% after 10 h. The initial CO conversion of H_2-pretreated 0.5Au-Fe catalyst is 100%, and the CO conversion was decreased with the time on stream. After 10 h, CO conversion was about 94%.

The stability test further evidenced the highest performance of H_2-pretreated 0.5Au-Fe catalyst (Figure 11). The XRD analysis of spent catalyst indicated that sintering of Au or Fe_2O_3 did not occur during the time on stream analysis

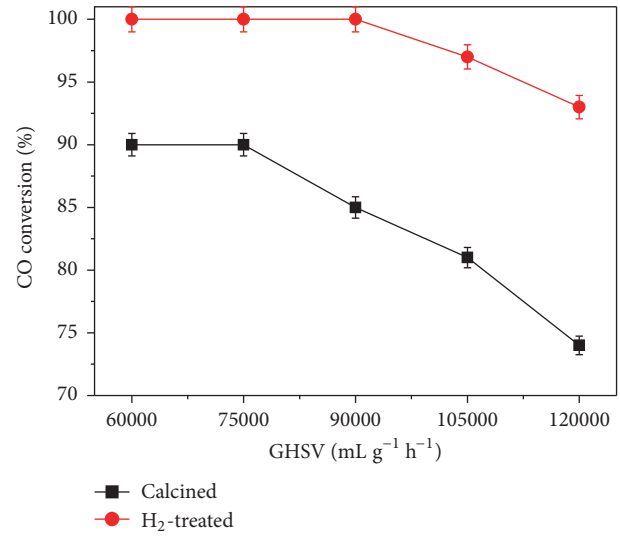

Figure 10: The influence of GHSV on CO conversion over the calcined and H_2-treated 0.5Au-Fe catalyst (reaction conditions: temperature 303 K; weight of catalyst 0.5 g; total flow rate 1000 mL min^{-1}; feed composition 100 ppm CO/air).

because the reaction temperature and reduction temperature were lower than the calcination temperature. The slight deactivation observed in the Au-Fe nanocomposite samples is probably due to deposition of carbonate and carbonyl species on the surface of the catalyst.

It is clear that Au-Fe composite samples possessed catalytically active species and they offer a high activity from the beginning and are stable during catalytic tests. The nature of Au and Fe_2O_3 species responsible for the observed activity could be explained on the basis of characterization results. It was widely reported that properties of catalysts, such as particle size, active metal dispersion, surface area, and strength of interaction, have a great influence on the redox properties and reactivity [50]. The behavior of Au supported catalysts was mainly attributed to the electronic interaction between the Au and support [51] as well as the contribution from H_2 pretreatment prior to the reaction.

It is clear that a dispute exists in the literature concerning the role of Fe_2O_3 support and active Au species in Au/Fe_2O_3

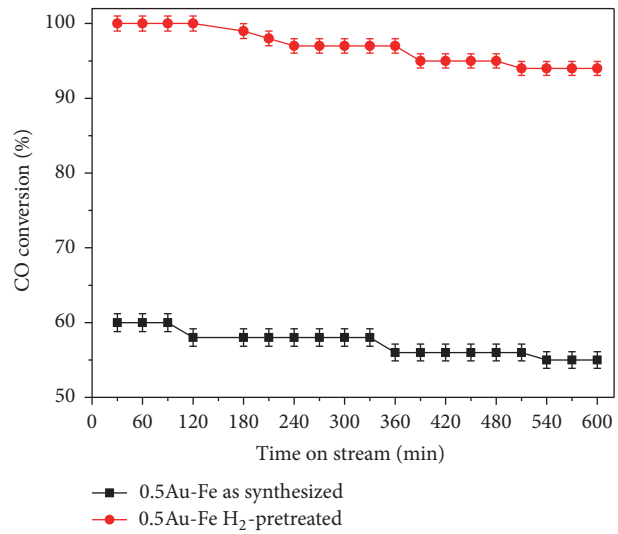

FIGURE 11: Time on stream analysis of 0.5Au-Fe catalysts (reaction conditions: weight of catalyst 0.5 g; total flow rate 1000 mL min^{-1}; feed composition: 100 ppm CO/air; T: 293 K; GHSV = 120,000 mL g^{-1} h^{-1}).

catalysts for CO oxidation. Liu et al. [52] reported that oxygen atoms of the Fe_2O_3 lattice do not participate in the reaction at room temperature. The catalytic oxidation takes place via the interaction of CO adsorbed on the surface of the Au particles and O_2 adsorbed on the adjacent oxygen vacancies on the surface of the support. However, Tripathy et al. [53] studied the CO oxidation using the microcalorimetry technique and concluded that the lattice oxygen of Fe_2O_3 does play an important role in the reaction. Later, Guczi et al. [54] proposed that the high activity of Au-Fe_2O_3 samples for CO oxidation was due to the high O_2 adsorption over the Fe_2O_3, which acted as the oxygen reservoir during the reaction. Okumura and Haruta [9] observed that Au metallic species in Au/α-Fe_2O_3 catalysts are very active. However, Hutchings et al. [10] and Khoudiakov et al. [11] reported that Au cation species in the Au/Fe_2O_3 catalysts are responsible for activity in CO oxidation. Park and Lee [12] also reported that oxidized gold species are more active than metallic Au. These authors indicated that reduction of Au oxide to metallic Au could be one of the reasons for the deactivation of Au/Fe_2O_3 catalysts in CO oxidation. In addition, they observed that Au oxide and iron oxide reduction peaks shifted to a higher temperature in the H_2-TPR patterns, indicating that the strong interaction between Au species and Fe_2O_3 support. Very recently, Luengnaruemitchai et al. [55] reported a decrease of CO conversion from 95% to 44% at 333 K after oxygen pretreatment of the catalyst. It was suggested that the reason for the decrease of activity is the formation of surface oxygen species on the Au surface after the catalyst was treated with oxygen at low temperatures [56]. As we know, the reaction of CO with O_2 requires both CO and O_2 to be adsorbed on the catalyst surface. However, the reaction temperature for CO oxidation is low (273 K to 333 K), so the surface oxygen species will not be desorbed at these temperatures, and the oxygen species at the surface were occupying reactive sites. Thus, the strongly adsorbed surface oxygen species blocks the adsorption and diffusion of weakly adsorbed surface oxygen resulting in a decrease of CO oxidation activity. For this reason, we pretreated Au-Fe catalysts with H_2 at 353 K for 1 h to remove surface oxygen species.

Okumura and Haruta [9] also indicated that spherical gold particles, which are strongly attached to the support by their flat planes, could be one of the reasons for their high activity in catalytic oxidation. Grunwaldt et al. [57] also made a very similar suggestion that the interaction of gold particles with the Fe_2O_3 support is physically and electronically strong because the shape of gold particles is spherical and flattened on one side. On the basis of catalyst preparation conditions adopted in our study and characterization results, we can suggest that Au^{3+} ions in the gold precursor deposited on the surface of the support and became $Au^{\delta+}$ due to the interaction between them. In case of catalysts which have lower Au loading (0.1 wt.% to 0.5 wt.%), the extent of interaction is high, which led to the formation of highly dispersive spherical Au particles (XRD, TEM, and XPS results). Further increase of Au loading to 1.0 wt.% resulted in the formation of agglomerated Au particles (XRD results). It was suggested that the agglomeration of Au particles could happen due to atom/clusters diffusion along the support and Ostwald ripening, where large particles grow at the expense of smaller particles due to the atomization and diffusion between particles [58].

The calcined Au-Fe nanocomposite samples contained both metallic Au and oxidic Au-Fe interactive species. It was already proven that both Au^{III} and Au^0 species are active for CO oxidation [59]. After the catalyst was exposed to CO/O_2 mixture, the $Au^{\delta+}/Au^0$ ratio was decreased and after sufficiently long exposure only metallic Au will remain. It appears that the decrease in the activity that we and other researchers [11] observed with just calcined catalysts is due to the Au^{III} to Au^0 transformation.

The superior catalytic activity of the 0.5Au-Fe catalyst could be explained as due to the formation of small Au-Fe particles dispersed on the support structure and also possessing of large surface area (Table 1). It was previously reported that the CO oxidation reaction normally takes place at the interface between gold cationic species and the iron sites [60]. The size of the interface between the Au particles and Fe_2O_3 is an important factor influencing the catalytic response of supported Au catalysts in reaction of CO oxidation [61]. It is generally accepted that the oxidation of CO over transition-metal oxides such as Fe_2O_3, MnO_2, and CuO follows a Mars-van Krevelen mechanism, in which lattice oxygen is involved in CO oxidation and the reduced surface of the catalyst is reoxidized by CO/O_2 feed mixture [62]. A high activity for CO oxidation can be achieved due to quick redox cycle through the spillover of reactive oxygen from the support to Au [63]. The XRD pattern of the spent 0.5Au-Fe catalyst (not shown) showed diffraction peaks due to hematite phase as a fresh sample, and no new diffractions peak due to Au oxides appeared. This observation clearly

indicated that the Au-Fe catalysts have not undergone any structural changes under adapted reaction conditions.

4. Conclusions

In summary, we have successfully synthesized a mesoporous α-Fe_2O_3 material by simple hydrothermal method and the obtained α-Fe_2O_3 was used to prepare Au-Fe nanocomposites with different Au loadings (0.1 to 1.0 wt.%). The calcined and H_2-pretreated Au-Fe nanocomposite samples showed a high catalytic activity for CO oxidation at low temperatures. CO was fully converted at reaction temperature as low as 313 K over the H_2-pretreated catalysts. Catalytic performance of Au-Fe nanocomposites depends strongly on Au loading, among which 0.5 wt.% Au displayed the best performance. Further increase of the Au loading resulted in a decrease of CO oxidation activity. The characterization results suggest that both metallic Au and partially oxidized Au species are responsible for the catalytic oxidation of CO in addition to the Au particle size. The mesoporous nature with high specific surface area of the Au-Fe nanocomposites is also a contributing factor for the observed high catalytic activity. The Au-Fe nanocomposites also showed good reproducibility and stability in CO oxidation. The Au-Fe nanocomposites showed higher CO oxidation activity than other Au supported catalysts reported in the literature mainly due to enhanced interaction between Au nanoparticles and the mesoporous Fe_2O_3 support.

Conflicts of Interest

The authors declare that there are no conflicts of interest regarding the publication of this paper.

Acknowledgments

This project was funded by the Deanship of Scientific Research (DSR) at King Abdulaziz University, Jeddah, under Grant no. 17/130/1435. The authors therefore acknowledge with thanks the DSR for the technical and financial support.

References

[1] G. J. Hutchings and J. K. Edwards, *Metal Nanoparticles and Nanoalloys*, vol. 3, 2012.

[2] R. F. Coburn, "Mechanisms of carbon monoxide toxicity," *Preventive Medicine*, vol. 8, no. 3, pp. 310–322, 1979.

[3] J. C. Amphlett, K. A. M. Creber, J. M. Davis, R. F. Mann, B. A. Peppley, and D. M. Stokes, "Hydrogen production by steam reforming of methanol for polymer electrolyte fuel cells," *International Journal of Hydrogen Energy*, vol. 19, no. 2, pp. 131–137, 1994.

[4] Y. Nishihata, J. Mizuki, T. Akao et al., "Self-regeneration of a Pd-perovskite catalyst for automotive emissions control," *Nature*, vol. 418, no. 6894, pp. 164–167, 2002.

[5] M. M. Schubert, S. Hackenberg, A. C. Van Veen, M. Muhler, V. Plzak, and J. Behm, "CO oxidation over supported gold catalysts—'Inert' and 'active' support materials and their role for the oxygen supply during reaction," *Journal of Catalysis*, vol. 197, no. 1, pp. 113–122, 2001.

[6] M. Haruta, N. Yamada, T. Kobayashi, and S. Iijima, "Gold catalysts prepared by coprecipitation for low-temperature oxidation of hydrogen and of carbon monoxide," *Journal of Catalysis*, vol. 115, pp. 301–309, 1989.

[7] K. Narasimharao, A. Al-Shehri, and S. Al-Thabaiti, "Porous Ag-Fe2O3 nanocomposite catalysts for the oxidation of carbon monoxide," *Applied Catalysis A: General*, vol. 505, pp. 431–440, 2015.

[8] R. Rioux, *Model Systems in Catalysis*, Springer Science Business, New York, NY, USA, November 2009.

[9] M. Okumura and M. Haruta, "Preparation of supported gold catalysts by liquid-phase grafting of gold acethylacetonate for low-temperature oxidation of CO and of H_2," *Chemistry Letters*, no. 4, pp. 396-397, 2000.

[10] G. J. Hutchings, M. S. Hall, A. F. Carley et al., "Role of gold cations in the oxidation of carbon monoxide catalyzed by iron oxide-supported gold," *Journal of Catalysis*, vol. 242, no. 1, pp. 71–81, 2006.

[11] M. Khoudiakov, M. C. Gupta, and S. Deevi, "Au/Fe_2O_3 nanocatalysts for CO oxidation: a comparative study of deposition-precipitation and coprecipitation techniques," *Applied Catalysis A: General*, vol. 291, no. 1-2, pp. 151–161, 2005.

[12] E. D. Park and J. S. Lee, "Effects of pretreatment conditions on CO oxidation over supported Au catalysts," *Journal of Catalysis*, vol. 186, pp. 1–11, 1999.

[13] A. Luengnaruemitchai, D. T. K. Thoa, S. Osuwan, and E. Gulari, "A comparative study of Au/MnO_x and Au/FeO_x catalysts for the catalytic oxidation of CO in hydrogen rich stream," *International Journal of Hydrogen Energy*, vol. 30, no. 9, pp. 981–987, 2005.

[14] S.-W. Cao, J. Fang, M. M. Shahjamali et al., "In situ growth of Au nanoparticles on Fe_2O_3 nanocrystals for catalytic applications," *CrystEngComm*, vol. 14, no. 21, pp. 7229–7235, 2012.

[15] P. Li and D. E. Miser, "The removal of carbon monoxide by iron oxide nanoparticles," *Applied Catalysis B: Environmental*, vol. 43, pp. 151–162, 2003.

[16] P. Llewellyn, *Adsorption by Powders and Porous Solids: Principles, Methodology and Applications*, 2014.

[17] H. Liang, K. Liu, and Y. Ni, "Synthesis of mesoporous α-Fe_2O_3 via sol–gel methods using cellulose nano-crystals (CNC) as template and its photo-catalytic properties," *Materials Letters*, vol. 159, pp. 218–220, 2015.

[18] S. G. Hosseini, R. Ahmadi, A. Ghavi, and A. Kashi, "Synthesis and characterization of α-Fe_2O_3 mesoporous using SBA-15 silica as template and investigation of its catalytic activity for thermal decomposition of ammonium perchlorate particles," *Powder Technology*, vol. 278, pp. 316–322, 2015.

[19] C. K. Costello, M. C. Kung, H. S. Oh, Y. Wang, and H. H. Kung, "Nature of the active site for CO oxidation on highly active Au/γ-Al_2O_3," *Applied Catalysis A: General*, vol. 232, pp. 159–168, 2001.

[20] M. C. Kung, R. J. Davis, and H. H. Kung, "Understanding au-catalyzed low-temperature CO oxidation," *Journal of Physical Chemistry C*, vol. 111, no. 32, pp. 11767–11775, 2007.

[21] Z. Zhong, J. Ho, J. Teo, S. Shen, and A. Gedanken, "Synthesis of porous α-Fe_2O_3 nanorods and deposition of very small gold particles in the pores for catalytic oxidation of CO," *Chemistry of Materials*, vol. 19, no. 19, pp. 4776–4782, 2007.

[22] S. N. Basahel, M. Mokhtar, E. H. Alsharaeh, T. T. Ali, H. A. Mahmoud, and K. Narasimharao, "Physico-chemical and catalytic properties of mesoporous CuO-ZrO_2 catalysts," *Catalysts*, vol. 6, no. 4, article 57, 2016.

[23] Y. Liu, L. Chen, J. Hu, J. Li, and R. Richards, "TiO_2 nanoflakes modified with gold nanoparticles as photocatalysts with high activity and durability under near UV irradiation," *Journal of Physical Chemistry C*, vol. 114, pp. 1641–1645, 2010.

[24] T. Fujitani and I. Nakamura, "Mechanism and active sites of the oxidation of CO over Au/TiO_2," *Angewandte Chemie—International Edition*, vol. 50, no. 43, pp. 10144–10147, 2011.

[25] T. V. Choudhary and D. W. Goodman, "Oxidation catalysis by supported gold nano-clusters," *Topics in Catalysis*, vol. 21, pp. 25–34, 2002.

[26] Y. P. He, Y. M. Miao, C. R. Li et al., "Size and structure effect on optical transitions of iron oxide nanocrystals," *Physical Review B - Condensed Matter and Materials Physics*, vol. 71, no. 12, Article ID 125411, 2005.

[27] H. Zhu, E. Zhu, G. Ou, L. Gao, and J. Chen, "Fe_3O_4-Au and Fe_2O_3-Au hybrid nanorods: layer-by-layer assembly synthesis and their magnetic and optical properties," *Nanoscale Research Letters*, vol. 5, no. 11, pp. 1755–1761, 2010.

[28] A. S. Reddy, C.-Y. Chen, C. C. Chen et al., "Synthesis and characterization of Fe/CeO_2 catalysts: epoxidation of cyclohexene," *Journal of Molecular Catalysis A: Chemical*, vol. 318, no. 1-2, pp. 60–67, 2010.

[29] K. S. W. Sing, D. H. Everett, R. A. W. Haul et al., "Reporting physisorption data for gas/solid systems with special reference to the determination of surface area and porosity (recommendations 1984)," *Pure and Applied Chemistry*, vol. 57, pp. 603–619, 1985.

[30] K. S. W. Sing, "Reporting physisorption data for gas/solid systems with special reference to the determination of surface area and porosity (provisional)," *Pure and Applied Chemistry*, vol. 54, pp. 2201–2218, 1982.

[31] J. Huang, W. L. Dai, and K. N. Fan, "Remarkable support crystal phase effect in Au/FeO_x catalyzed oxidation of 1,4-butanediol to γ-butyrolactone," *Journal of Catalysis*, vol. 266, pp. 228–235, 2009.

[32] M. S. Chen and D. W. Goodman, "The structure of catalytically active gold on titania," *Science*, vol. 306, no. 5694, pp. 252–255, 2004.

[33] S. Arrii, F. Morfin, A. J. Renouprez, and J. L. Rousset, "Oxidation of CO on gold supported catalysts prepared by laser vaporization: direct evidence of support contribution," *Journal of the American Chemical Society*, vol. 126, no. 4, pp. 1199–1205, 2004.

[34] C. L. Peza-Ledesma, L. Escamilla-Perea, R. Nava, B. Pawelec, and J. L. G. Fierro, "Supported gold catalysts in SBA-15 modified with TiO_2 for oxidation of carbon monoxide," *Applied Catalysis A: General*, vol. 375, no. 1, pp. 37–48, 2010.

[35] H. Y. Lin and Y. W. Chen, "Low-temperature CO oxidation on Au/Fe_xO_y catalysts," *Industrial & Engineering Chemistry Research*, vol. 44, no. 13, pp. 4569–4576, 2005.

[36] W. S. Epling, G. B. Hoflund, J. F. Weaver, S. Tsubota, and M. Haruta, "Surface characterization study of Au/α-Fe_2O_3 and Au/Co_3O_4 low-temperature CO oxidation catalysts," *The Journal of Physical Chemistry*, vol. 100, pp. 9929–9934, 1996.

[37] C. R. Brundle, "Oxygen adsorption and thin oxide formation at iron surfaces: an XPS/UPS study," *Surface Science*, vol. 66, no. 2, pp. 581–595, 1977.

[38] J. F. Moulder, W. F. Stickle, P. E. Sobol, and K. D. Bomben, *Handbook of X-Ray Photoelectron Spectroscopy*, Perkin-Elmer, Waltham, Mass, USA, 1992.

[39] B. Aeijelts Averink Silberova, G. Mul, M. Makkee, and J. A. Moulijn, "DRIFTS study of the water-gas shift reaction over Au/Fe_2O_3," *Journal of Catalysis*, vol. 243, no. 1, pp. 171–182, 2006.

[40] S. A. C. Carabineiro, N. Bogdanchikova, P. B. Tavares, and J. L. Figueiredo, "Nanostructured iron oxide catalysts with gold for the oxidation of carbon monoxide," *RSC Advances*, vol. 2, no. 7, pp. 2957–2965, 2012.

[41] A. Venugopal and M. S. Skurrell, "Low temperature reductive pretreatment of Au/Fe_2O_3 catalysts, TPR/TPO studies and behaviour in the water–gas shift reaction," *Applied Catalysis A: General*, vol. 258, no. 2, pp. 241–249, 2004.

[42] A. S. K. Hashmi and G. J. Hutchings, "Gold catalysis," *Angewandte Chemie—International Edition*, vol. 45, no. 47, pp. 7896–7936, 2006.

[43] K. Qian, W. Zhang, H. Sun et al., "Hydroxyls-induced oxygen activation on 'inert' Au nanoparticles for low-temperature CO oxidation," *Journal of Catalysis*, vol. 277, no. 1, pp. 95–103, 2011.

[44] N. W. Cant, P. C. Hicks, and B. S. Lennon, "Steady-state oxidation of carbon monoxide over supported noble metals with particular reference to platinum," *Journal of Catalysis*, vol. 54, no. 3, pp. 372–383, 1978.

[45] Tana, F. Wang, H. Li, and W. Shen, "Influence of Au particle size on Au/CeO_2 catalysts for CO oxidation," *Catalysis Today*, vol. 175, no. 1, pp. 541–545, 2011.

[46] W. Zhang, X. Lu, W. Zhou, F. Wu, and J. Li, "Mesoporous iron oxide-silica supported gold catalysts for low-temperature CO oxidation," *Chinese Science Bulletin*, vol. 59, pp. 4008–4013, 2014.

[47] N. Weiher, E. Bus, L. Delannoy et al., "Structure and oxidation state of gold on different supports under various CO oxidation conditions," *Journal of Catalysis*, vol. 240, no. 2, pp. 100–107, 2006.

[48] A. A. Herzing, C. J. Kiely, A. F. Carley, P. Landon, and G. J. Hutchings, "Identification of active gold nanoclusters on iron oxide supports for CO oxidation," *Science*, vol. 321, no. 5894, pp. 1331–1335, 2008.

[49] P. Liu and J. Rodriguez, "Water-gas-shift reaction on metal nanoparticles and surfaces," *The Journal of Chemical Physics*, vol. 126, pp. 164705–164712, 2007.

[50] N. A. Hodge, C. J. Kiely, R. Whyman et al., "Microstructural comparison of calcined and uncalcined gold/iron-oxide catalysts for low-temperature CO oxidation," *Catalysis Today*, vol. 72, no. 1-2, pp. 133–144, 2002.

[51] W. Deng, C. Carpenter, N. Yia, and M. F. Stephanopoulos, "Comparison of the activity of Au/CeO_2 and Au/Fe_2O_3 catalysts for the CO oxidation and the water-gas shift reactions," *Topics in Catalysis*, vol. 44, no. 1, pp. 199–208, 2007.

[52] H. Liu, A. I. Kozlov, A. P. Kozlova, T. Shido, and Y. Iwasawa, "Active oxygen species and reaction mechanism for low-temperature CO oxidation on an Fe_2O_3-supported Au catalyst prepared from $Au(PPh_3)(NO_3)$ and as-precipitated iron hydroxide," *Physical Chemistry Chemical Physics*, vol. 1, no. 11, pp. 2851–2860, 1999.

[53] A. K. Tripathy, V. S. Kamble, and N. M. Gupta, "Microcalorimetry, adsorption, and reaction studies of CO, O_2, and $CO+O_2$ over Au/Fe_2O_3, Fe_2O_3, and polycrystalline gold catalysts," *Journal of Catalysis*, vol. 187, pp. 332–342, 1999.

[54] L. Guczi, D. Horváth, Z. Pászti, and G. Petõ, "Effect of treatments on gold nanoparticles: Relation between morphology,

electron structure and catalytic activity in CO oxidation," *Catal Today*, vol. 72, no. 1-2, pp. 101–105, 2002.

[55] A. Luengnaruemitchai, K. Srihamat, C. Pojanavaraphan, and R. Wanchanthuek, "Activity of Au/Fe_2O_3-TiO_2 catalyst for preferential CO oxidation," *International Journal of Hydrogen Energy*, vol. 40, no. 39, pp. 13443–13455, 2015.

[56] Z. Qu, W. Huang, S. Zhou, H. Zheng, X. Liu, and M. Cheng, "Enhancement of the catalytic performance of supported-metal catalysts by pretreatment of the support," *Journal of Catalysis*, vol. 234, pp. 33–36, 2005.

[57] J.-D. Grunwaldt, M. Maciejewski, O. S. Becker, P. Fabrizioli, and A. Baiker, "Comparative study of Au/TiO_2 and Au/ZrO_2 catalysts for low-temperature CO oxidation," *Journal of Catalysis*, vol. 186, no. 2, pp. 458–469, 1999.

[58] C. C. Chusuei, X. Lai, K. Luo, and D. W. Goodman, "Modeling heterogeneous catalysts: metal clusters on planar oxide supports," *Topics in Catalysis*, vol. 14, no. 1–4, pp. 71–83, 2000.

[59] A. M. Visco, F. Neri, G. Neri, A. Donato, C. Milone, and S. Galvagno, "X-ray photoelectron spectroscopy of Au/Fe_2O_3 catalysts," *Physical Chemistry Chemical Physics*, vol. 1, no. 11, pp. 2869–2873, 1999.

[60] R. E. Ramírez-Garza, B. Pawelec, T. A. Zepeda, and A. Martínez-Hernández, "Total CO oxidation over Fe-containing Au/HMS catalysts: effects of gold loading and catalyst pretreatment," *Catalysis Today*, vol. 172, no. 1, pp. 95–102, 2011.

[61] T. Hayashi, K. Tanaka, and M. Haruta, "Selective vapor-phase epoxidation of propylene over Au/TiO_2 catalysts in the presence of oxygen and hydrogen," *Journal of Catalysis*, vol. 178, no. 2, pp. 566–575, 1998.

[62] S. Minicò, S. Scirè, C. Crisafulli, and S. Galvagno, "Influence of catalyst pretreatments on volatile organic compounds oxidation over gold/iron oxide," *Applied Catalysis B: Environmental*, vol. 34, no. 4, pp. 277–285, 2001.

[63] L. Li, A. Wang, B. Qiao et al., "Origin of the high activity of Au/FeO_x for low-temperature CO oxidation: direct evidence for a redox mechanism," *Journal of Catalysis*, vol. 299, pp. 90–100, 2013.